

Military Technical College  
Cairo, Egypt



12<sup>th</sup> International Conference  
on Applied Mechanics and  
Mechanical Engineering (AMME)

## SMART FLUID DAMPER MODELS APPLIED TO VEHICLES VIBRATION CONTROL

El-Demerdash<sup>\*</sup> S., El-Butch<sup>\*\*</sup> A., Rabieh<sup>\*\*\*</sup> E., and El kafafy<sup>\*\*\*\*</sup> M.

### ABSTRACT

Electro-and magneto-rheological fluids are smart, synthetic fluids changing their viscosity from liquid to semi-solid state within milliseconds if a sufficient strong electric or magnetic field is applied. When used in suitable devices, they offer the innovative potential of very fast; adaptively interface between mechanical devices and electronic control units. This paper gives an overview on the basic properties of electro and magneto-rheological fluids and discusses various phenomenological models for rheological fluid dampers in vibratory systems. The dynamic response of a quarter-car model with MR- suspension damper is introduced and compared with one uses a conventional viscous damper.

### KEY WORDS

Electro-and Magneto-Rheological fluid devices, Phenomenological models, Numerical simulation, Passive suspension.

---

\* Prof. Automotive and Tractors Engineering Dept.

\*\* Asso. Prof., Mechanical Design Dept.

\*\*\* Asso. Prof., Mechanical Design Dept.

\*\*\*\* Post Graduated Student

## 1. INTRODUCTION

Electro-(ER) and magneto-rheological (MR) fluids are colloidal suspensions, which exhibit large reversible changes in flow properties such as the apparent viscosity when subjected to sufficiently strong electric and magnetic fields respectively, [1]. They usually consist of micron-sized polarisable or magnetsable solid particles dissolved in a non-conducting liquid like mineral or silicon oil. The composition of ER and MR fluids exhibits a broad diversity concerning solvent, solute and additives. Recently, ER and MR fluids have attracted considerable interest due to their wide range of use in vibration dampers for vehicle suspension systems ([2],[3],[4],[5]) machinery mounts or even seismic protection of structures [6],[7].

Their stiffness and damping capabilities can be adjusted very quickly by applying a suitable electric or magnetic field. In order to achieve desirable control performance, it is necessary to have an accurate damping force behavior of ER or MR damper.

ER and MR fluid dampers enable active and semi active vibration control systems with reaction times in the range of milliseconds and, additionally, low power requirements when using MR fluids. Due to their rather simple mechanical design which involves only few moving parts they ensure high technical reliability and exhibit almost no wear. Thus, continuously adjustable ER and MR fluid devices offer the fast controllable interfaces between mechanical components and electronic control units. In this paper, seven phenomenological models for ER and MR fluid devices are presented. Their validity is discussed as far as comparisons with previously published experimental data [8] have been introduced. Finally, the dynamic response of a quarter-car model with MR- suspension damper is introduced and compared with one using a conventional viscous damper.

## 2. DAMPER MODELS

### 2.1 Bingham Model, [9]

Most commonly, the Bingham plastic model describes the behavior of ER and MR fluids. An ideal Bingham body behaves as a solid until a minimum yield stress  $\tau_y$  is exceeded and then exhibits a linear relation between the stress and the rate of shear or deformation. Accordingly, the shear stress  $\tau$  developed in the fluid is given by;

$$\tau = \tau_y \cdot \text{sgn}(\dot{\gamma}) + \eta \dot{\gamma} \quad (1)$$

Where  $\dot{\gamma}$  is the strain rate and  $\eta$  denotes the plastic viscosity of the fluid, i.e., the (Newtonian) viscosity at zero field. In order to characterize the ER damping mechanism Stanway, et al [9] proposed a mechanical model, commonly referred to as Bingham model. In this model, the damping force of the rheological damper can be described as a combination of Coulomb friction force in parallel with viscous damping force as shown in Fig. 1. The total damping force is given as;

$$F - f_0 = c_0 \dot{\chi} + F_y \text{sgn}(\dot{\chi}) \quad (2)$$

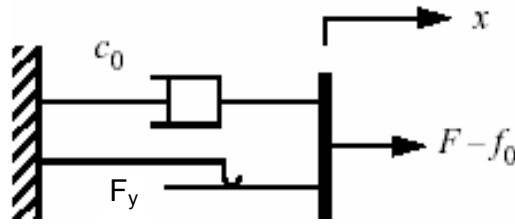


Fig.1. Bingham model

$F$  is a viscous damping force,  $c_o$  is post-yield plastic viscous damping coefficient,  $F_y$  is coulomb friction force (yield force),  $\dot{x}$ , is the velocity across the damper and  $f_o$  is the damper friction force due to seals and measurement bias. The damping coefficient  $c_o$  and the yield force  $F_y$  are related to the fluid's viscosity and the filled dependent yield stress, respectively. The parameters of this model are chosen to be;  $c_o = 800000$  N.s/m,  $F_y = 160000$  N, and  $f_o = -1449$  N,

Fig.2. provides the damping force against the velocity and displacement using the Bingham model and the previously published experimental results [8]. As shown, this model is essentially the same as the quasi-static models. Therefore, it is not surprising that the MR-damper force–displacement behavior is reasonably modeled. However, the nonlinear force-velocity behavior is not captured where the Bingham model cannot captured the hysteretic loop in the pre-yield region. Therefore, the Bingham model accounts for electro- and magnetorheological fluid behavior beyond the yield point, i.e. for fully developed fluid flow or sufficient high shear rates. However, it assumes that the fluid remains rigid in the pre-yield region. Thus, Bingham model does not describe the fluid's elastic properties at small deformation and low shear rates, which is necessary for dynamic applications.

### 2.2 Herschel-Bulkley Visco-Plasticity Model, [8]

The fluid post-yield viscosity is assumed constant in the Bingham model, therefore, the shear thinning effect of the MR-fluid is not captured in the post-yield region. The Herschel-Bulkley visco-plastic model can be employed to accommodate this effect. In this model, the constant post-yield viscosity in the Bingham model is replaced with a power law model dependent on shear strain rate, therefore,

$$\tau = \left( \tau_y + k |\dot{\gamma}|^{\frac{1}{M}} \right) \text{sgn} (\dot{\gamma}) \tag{3}$$

where  $M$  and  $K$  are positive constants. Comparing Eq. (1) with Eq. (3) the equivalent plastic viscosity of the Herschel-Bulkly model is;

$$\eta_e = k |\dot{\gamma}|^{\frac{1}{M} - 1} \tag{4}$$

Eq. (4) indicates that the equivalent plastic viscosity,  $\eta_e$ , decreases as the shear strain rate  $\dot{\gamma}$  increase when  $M > 1$  (shear thinning). Furthermore, this model can also be used to describe the fluid shear thickening effect when  $M < 1$ . The Herschel-Bulkley model reduces to Bingham model when  $M = 1$ , therefore  $\eta = k$ . The total damping force is given from the following equation

The total damping force is given from the following equation

$$F - f_0 = (k |\dot{x}|^{\frac{1}{M}} + F_y) \text{sgn}(\dot{x}) \quad (5)$$

The parameters of this model are chosen to be  $k=250000$ ,  $F_y=160000$  N,  $f_0 = -1449$  N, and  $M = 1.9$

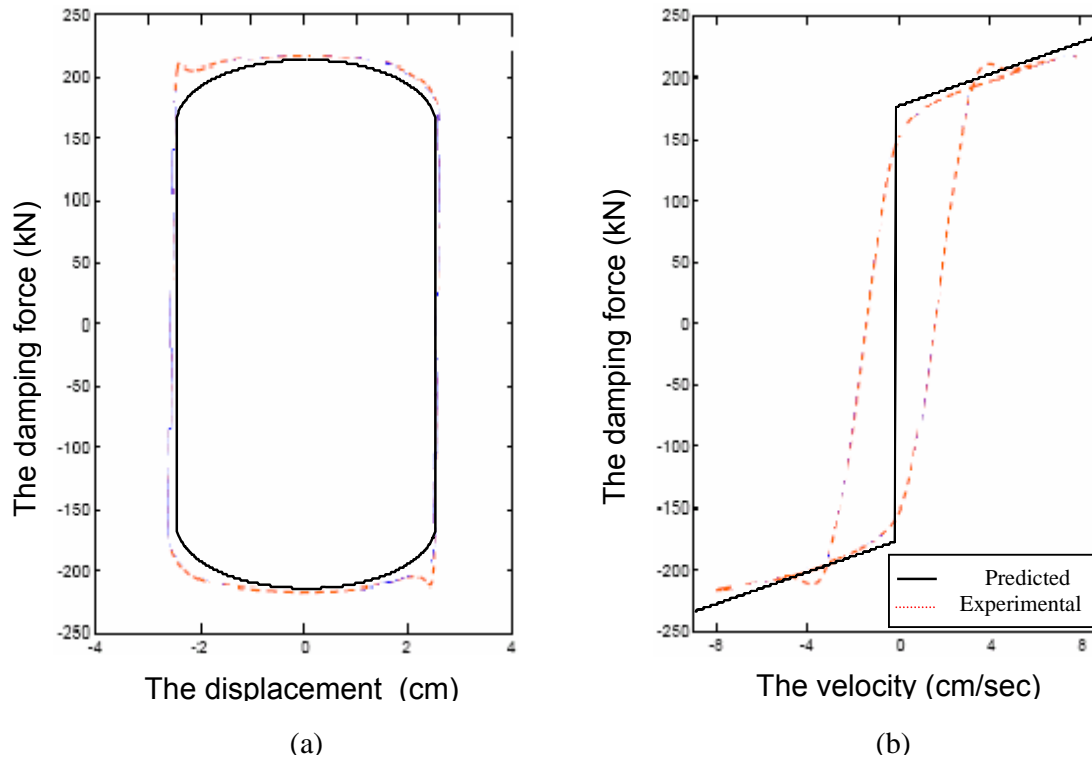


Fig.2. Comparison between the experimental [8] and predicted responses using the Bingham model: (a) force vs. displacement, and (b) force vs. velocity.

Fig.3. provides a comparison between the Herschel-Bulkley model and the experimental results, [8]. The Herschel-Bulkley model can capture the shear thinning effect of the MR-fluid damper as shown in the force–velocity diagram in the post-yield region where the viscosity decreases as the velocity increases. However, the force–displacement result nearly the same as Bingham model.

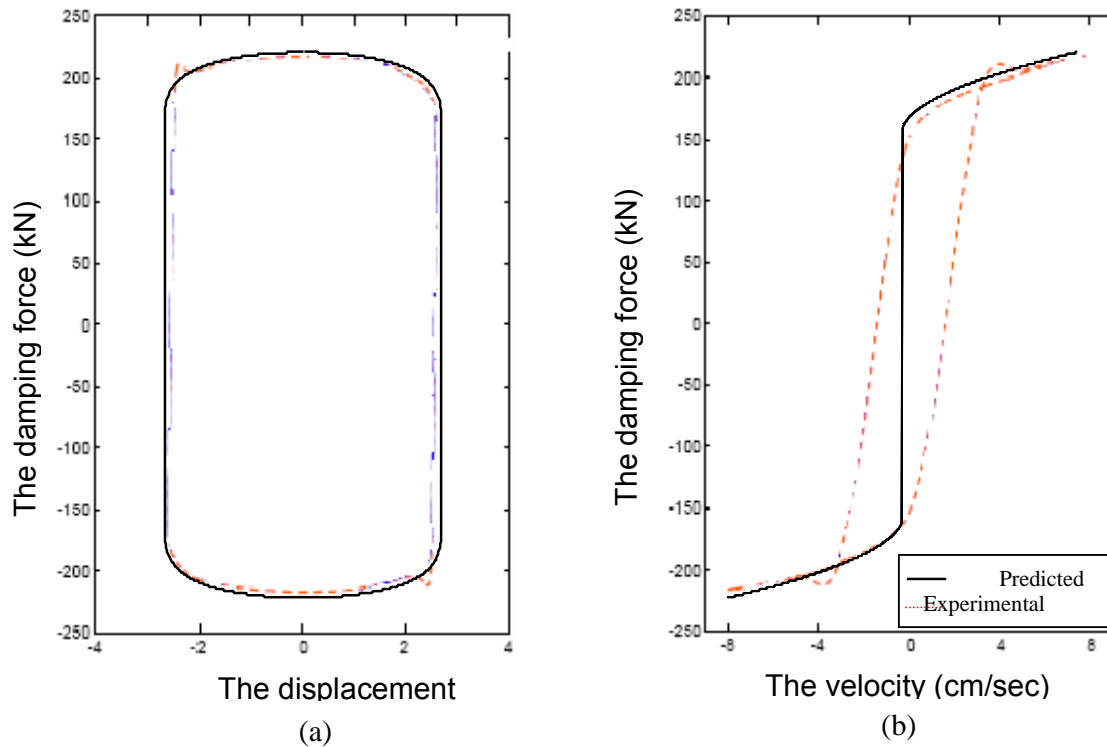


Fig.3. Comparison between the experimental [8] and predicted responses using the Herschel-Bulkely model: (a) force vs. displacement; (b) force vs. velocity

**2.3-Hysteretic Bingham Plastic Model, [10]**

By considering the excitation variables and appropriate parameters to the hyper tangent function, the pre-yield hysteresis of the MR-damper is presented. A modified Bingham plastic model for the MR-damper can be expressed by substituting a hysteresis loop shape function,  $S_h(x, \dot{x})$ , for the sign function,  $\text{sgn}(\dot{x})$ , of the Bingham-plastic model in equation (2). Fig.4. shows the elements of the hysteretic Bingham plastic model.

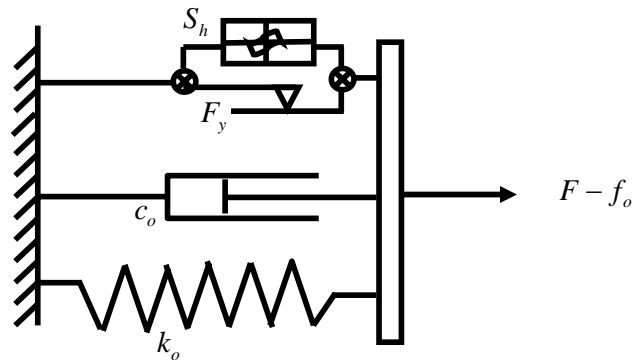


Fig.4. Hysteretic Bingham model

The total damping force is given from the following equation;

$$F - f_o = c_o \dot{x} + k_o x + F_y \tanh \left\{ \left( \dot{x} + \lambda_1 x \right) \lambda_2 \right\} \tag{6}$$

where

- $c_o$  Post-yield damping constant [N.s/m]
- $k_o$  The stiffness due to gas pressure in the accumulator [N/m]
- $F_y$  Coulomb friction force (yield force) [N]
- $\lambda_1, \lambda_2$  Parameters that account for the width and slope of the pre-yield hysteresis loop.

It is noted that, the larger value of the parameter  $\lambda_1$ , leads to the wider the hysteresis loop. In addition, a larger value of the parameter  $\lambda_2$  increases the slope of the pre-yield hysteresis loop.

The parameters for this model are chosen to be;

$$c_o = 643230 \text{ N.s/m}, k_o = 6000 \text{ N/m}, F_y = 180000 \text{ N}, f_o = -15000 \text{ N}, \lambda_1 = 0.7, \text{ and } \lambda_2 = 100.$$

Fig.5. provides a comparison between the Hysteretic Bingham model and the experimental results [8]. As shown in the figure, the hysteresis loop in the pre-yield region in the force–velocity plot is reasonably captured by the hysteretic Bingham model with the hysteretic shape function  $S_h(x, \dot{x})$ . The force roll off in the low velocity region is reasonably captured. However, the post-yield region is not well captured, where the clockwise loops at the velocity extremes, due to the stick phenomena and the inertial effect, are not captured. The force-displacement plot is reasonably presented as it is shown in the Fig. 5. To accommodate the stick phenomena and the inertial effect of the MR-fluid, a mass element  $m$  is added to the hysteretic Bingham model as shown in Fig.6.

The total damping force is;

$$F - f_o = c_o \dot{x} + k_o x + F_y \tanh \left\{ (\dot{x} + \lambda_1 x) \lambda_2 \right\} + m \ddot{x} \quad (7)$$

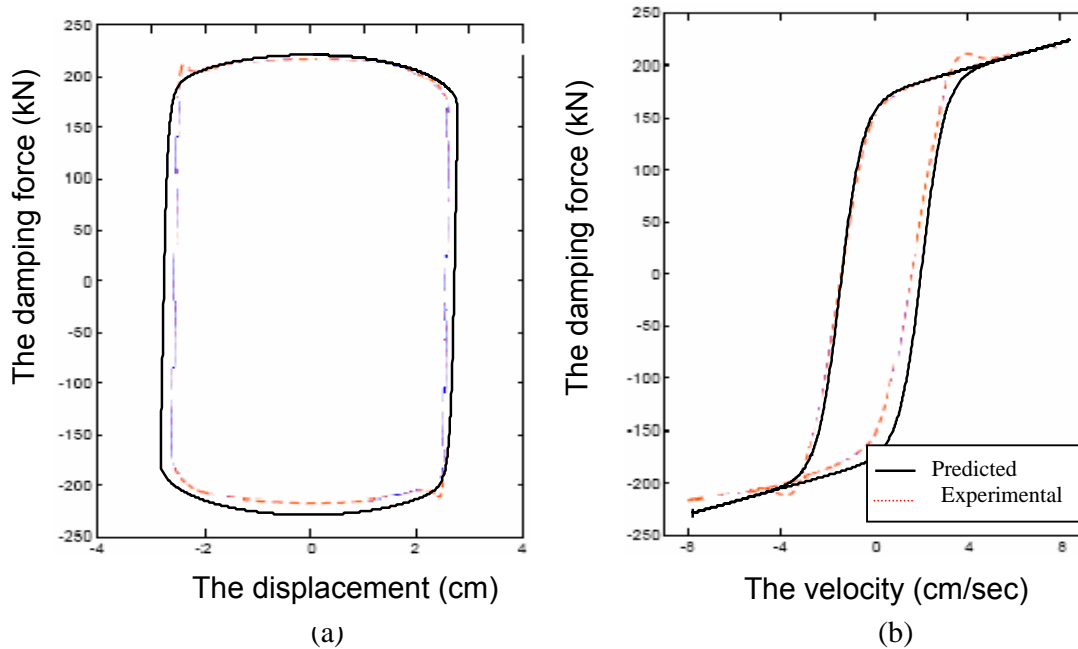


Fig.5. Comparison between the experimental, [8] and predicted responses using the hysteretic Bingham model: (a) force vs. displacement; (b) force vs. velocity

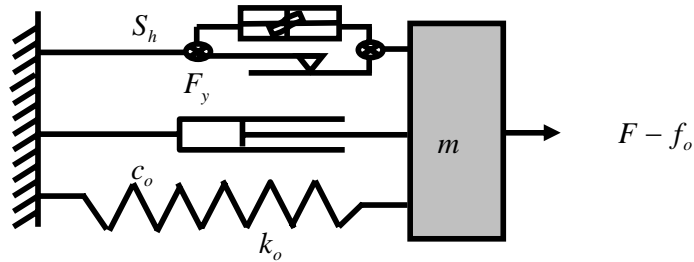


Fig.6. Hysteretic Bingham model with mass element

Where  $m$  equivalent mass which represents the MR- fluid stick and inertial effect (kg)

$\ddot{x}$  the damper acceleration (m/sec<sup>2</sup>)

The parameters are taken as the same in the pervious model with  $m = 14424$  kg.

As shown in Fig. 7, the hysteretic Bingham model with mass element has an improvement on modeling the two clockwise loops at the velocity extremes.

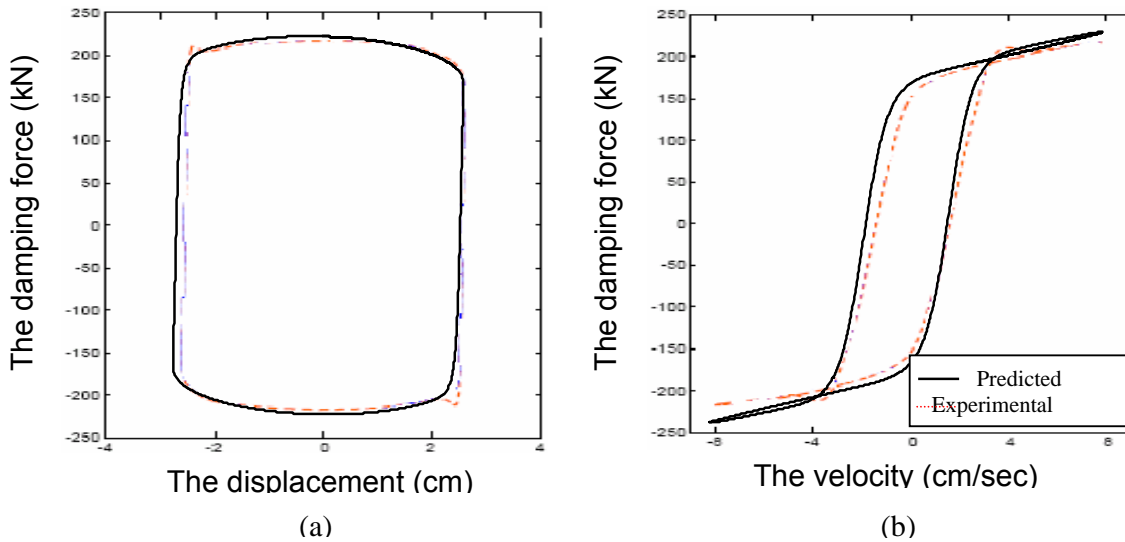


Fig. 7. Comparison between the experimental, [8] and predicted responses using the hysteretic Bingham with mass element model: (a) force vs. displacement; (b) force vs. velocity

**2.4-Bouc-Wen Model, [11]**

In their survey, Spencer, et al, [11] presented what so-called Bouc-Wen model in order to characterize the behavior of a MR-fluid damper. The concept is based on an approach due to Wen [12]. A mechanical analogy of the model is shown in Fig. 8.

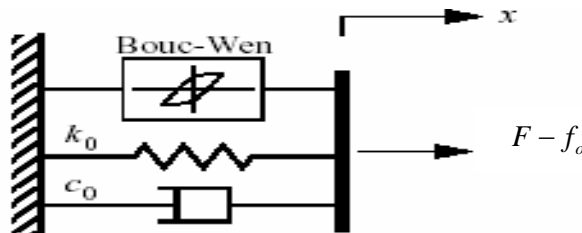


Fig.8. Bouc-Wen model

The hysteretic of damping force of the Bouc-Wen model can be given by;

$$F - f_o = c_o \dot{x} + k_o x + \alpha z \tag{8}$$

Where the hysteretic component z satisfies;

$$\dot{z} = -\gamma |\dot{x}| z |z|^{n-1} - \beta \dot{x} |z|^n + \delta \dot{x} \tag{9}$$

Where,

$F$  is the damping force (N) ,  $c_o$  viscous damping coefficient (N.s/m)

$k_o$  is the stiffness due to the presence of an accumulator in the considered damper and rheological fluid compressibility (N/m)

By adjusting the parameter values  $\beta$  ,  $\alpha$  ,  $\delta$  ,  $\gamma$  , and  $n$  , it is possible to control the force-velocity characteristic. In the above expression;  $\alpha$  and  $\delta$  are the strong functions of the applied magnetic field, and related to the height, width and slope of the pre-yield hysteresis loop. On other hand,  $\beta$  ,  $\gamma$  , and  $n$  give the basic configuration of the hysteresis loop, [10]. The parameters of this model are;

$$c_o = 643230 \text{ N.s/m}, \quad k_o = 279.14 \text{ N/m}, \alpha = 472710 \text{ N}, \quad \gamma = 5100.7 \text{ m}^{-1}$$

$$\beta = 150 \text{ m}^{-1}, \quad n = 2.2021, \quad f_o = -1449.3 \text{ N}, \text{ and } \delta = 550.57 \text{ m}^{-1}$$

Fig.9. provides a comparison between the Bouc-Wen model and the experimental published results, [8]. As shown in the force–velocity curve, this model is not capture the force roll-off in the low velocity region, as well as the two clockwise loops at the velocity extremes due to the stick phenomena and inertial effect. However, the force–displacement result is reasonably represented.

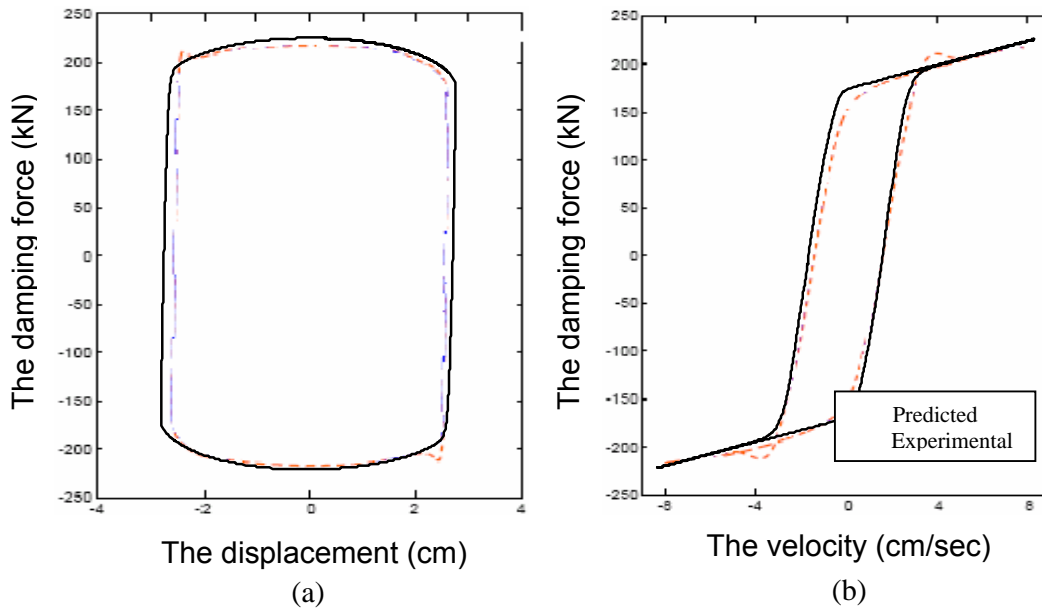


Fig.9. Comparison between the experimental [8] and predicted responses using Bouc-Wen model: (a) force vs. displacement; (b) force vs. velocity

**2.5. Bouc-Wen Model with Mass Element, [8]**

To accommodate the inertial effect, a mass element is added to the simple Bouc-Wen model as shown in Fig. 10. The total damping force will be;

$$F - f_o = c_o \dot{x} + k_o x + \alpha z + m \ddot{x} \tag{10}$$

The parameters of the Bouc-Wen model with mass element are taken to be the same as in the pervious section with a mass of ( $m = 14424$  kg).

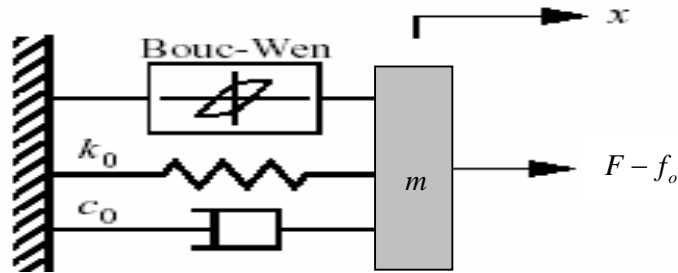


Fig.10. Bouc-Wen model with mass element

As shown in the Fig. 11, the simple Bouc-Wen model with mass element has an improvement on modeling the two clockwise loops at the velocity extremes. However, it fails to portray the force roll-off at low velocities.

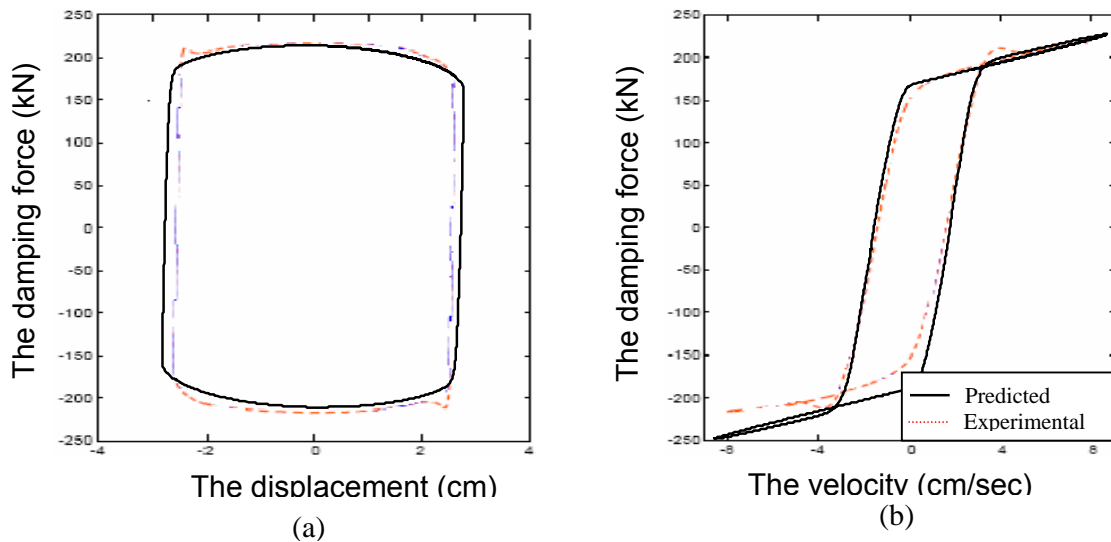


Fig.11. Comparison between the experimental [8] and predicted responses using Bouc-Wen model with mass element: (a) force vs. displacement; (b) force vs. velocity

**2.6. Modified Bouc-Wen Model, [11]**

For better prediction of the response of the MR-damper in the region of the yield point, Spencer et al, [11], proposed an extension of the Bouc-Wen model, which is depicted in Fig. 12. To obtain the governing equations for this model, consider only



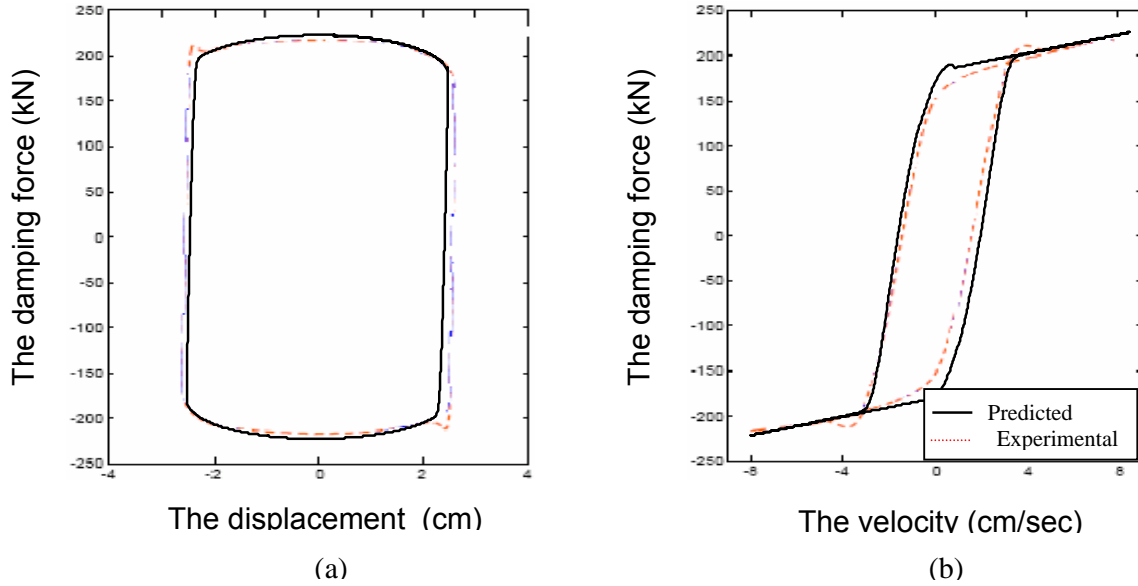


Fig.13. Comparison between the experimental [8] and predicted responses using the modified Bouc-Wen model: (a) force vs. displacement; (b) force vs. velocity.

Fig.13. shows a comparison between the predicted and experimental results in [8]. As shown in the figure, this mechanical model has only a slight improvement over the simple Bouc-Wen models in modeling the force roll-off at low velocity. One of the important advantages, which account for this model, that the parameters of this model are generalized for the fluctuation in the magnetic field. This means that, the Basic parameters are given as a function of the applied voltage and hence they are considered as a function of the magnetic field. This advantage makes this model to be more useful to be used for designing the control strategies of the system, which utilizes the MR-damper. This damper requires the magnetic field continuously to be vary based on the measured response of the attached system. Spencer, [11] found that,  $\alpha$  ,  $c_1$ , and,  $c_o$  are the more sensitive parameters to the magnetic field. Therefore, these parameters are assumed to be depending linearly on the voltage ( $v$  ) applied to the system, i.e.

$$\alpha = \alpha (U) = \alpha_a + \alpha_b U \tag{14}$$

$$c_1 = c_1 (U) = c_{1a} + c_{1b} U \tag{15}$$

$$c_o = c_o (U) = c_{oa} + c_{ob} U \tag{16}$$

Where  $U$  is governed by;

$$\dot{U} = - \sigma (U - v) \tag{17}$$

The first order filter given by Eq. (17) was introduced to allow for the fluid's dynamics of reaching rheological equilibrium. If the mass element is added to the modified Bouc-Wen model, the clockwise loops at the velocity extremes are represented as it is shown in Fig. (14). The mass will be taken to be ( $m = 14929$  kg).

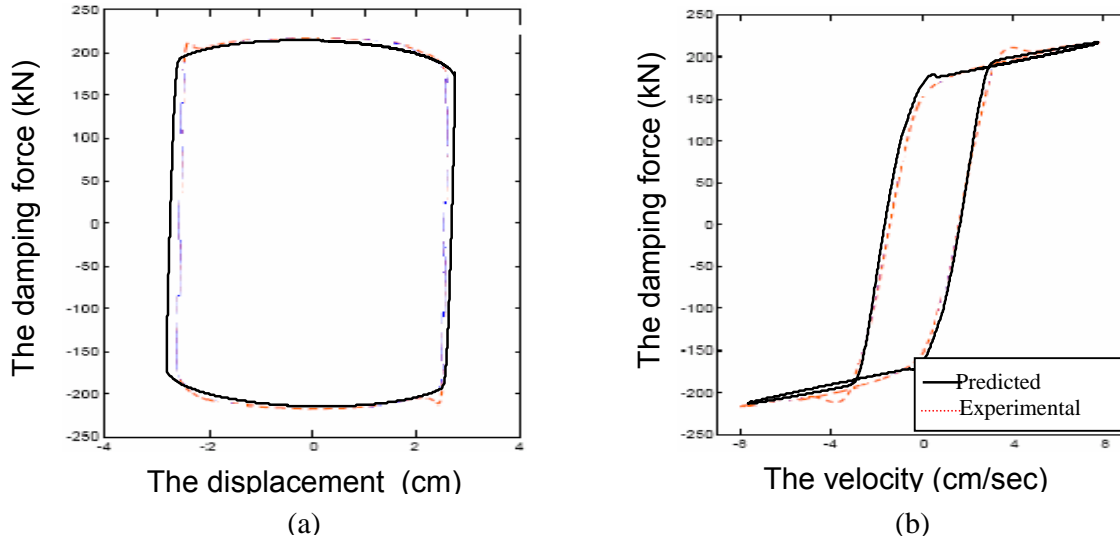


Fig.14. Comparison between the experimental, [8] and predicted responses using the modified Bouc-Wen model with mass element: (a) force vs. displacement; (b) force vs.

**2.7. Bouc-Wen model with mass element and variable damping, [8]**

This model is proposed by Guaugqiang [8], which considers the MR fluid phenomenon, as well as inertial and shears thinning effects. The schematic of the model is shown in the Fig. (15).

The damper force is given by;

$$F - f_0 = \alpha Z + k x + c(\dot{x})\dot{x} + m \ddot{x} \tag{18}$$

Where the evolutionary variable  $Z$  is governed by equation (9), and  $c(\dot{x})$  is the post yield plastic damping coefficient to describe the MR-fluid shear thinning effect which results in the force roll-off of the damping resisting force in low velocity region.

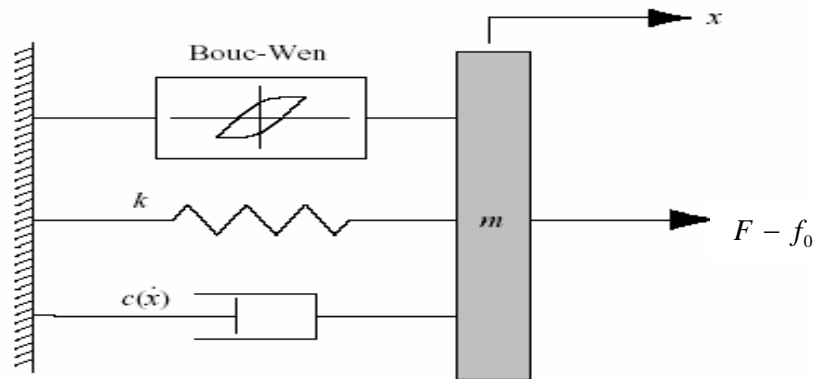


Fig.15. Proposed phenomenological model considering MR fluid stick phenomenon, as well as inertial and shear thinning effects.

The damping coefficient  $c(\dot{x})$  is defined as a mono-decreasing function with respect to the absolute velocity  $|\dot{x}|$ . In this model, the post yield-damping coefficient is assumed to have the form;

$$c(\dot{x}) = a_1 e^{-(a_2 |\dot{x}|)^{p_1}} \tag{19}$$

Where  $a_1$ ,  $a_2$ , and  $p_1$  are positive constants. The mass element  $m$  is employed to phenomenologically emulate the MR fluid stick phenomenon and fluid inertial effect. The parameters of this model are chosen to be:

$$a_1 = 3308891 \text{ N.s/m}, k = 486250 \text{ N/m}, \alpha = 927570 \text{ N}, \gamma = 31778 \text{ m}^{-1}$$

$$\beta = 21.637 \text{ m}^{-1}, n = 2.7755, f_o = -1377.32 \text{ N}, \text{ and } \delta = 217.27 \text{ m}^{-1}$$

$$a_2 = 24.9054 \text{ sec/m}, m = 14929 \text{ kg}, \text{ and } p_1 = 0.5403.$$

Figure (16) provides a comparison between the predicted and experimental obtained results [8]. As shown in the figure, it can be readily seen that this model predicts the damper behavior well in all region, including the force roll-off at low velocities, and the two clockwise loops at velocity extremes.

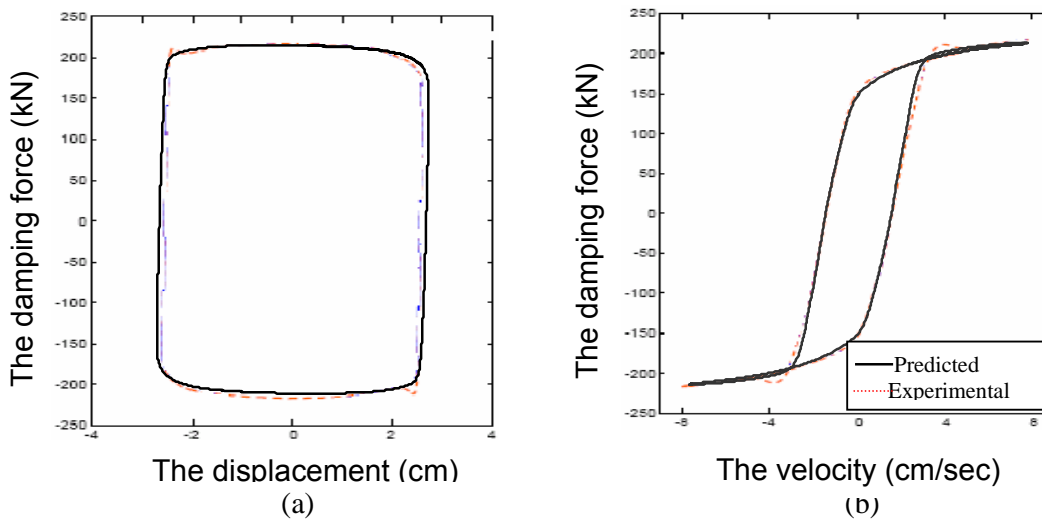


Fig.16. Comparison between the experimental, [8] and predicted responses using Bouc-Wen model with mass element and mono-decreasing damping function: (a) force vs. displacement; (b) force vs. velocity

### 3. SUMMARY

The hysteresis behavior of the MR-damper was characterized using damping force models. The Bingham plastic model fairly well describes post-yield force, but can not capture the hysteresis force behavior in the pre-yield region and the shear thinning effect. The Herschel-Bulekly model gives the same trend as the Bingham model, but it gives the shear thinning effect, which can appear in the force roll-off at the low velocity region. On the other hand, the remaining models beginning with hysteretic Bingham model well represent both the pre-yield and post-yield forces. When the mass element is included to the model, the post-yield region is captured well where the clockwise loops at the velocity extremes due to the stick phenomenon and the inertial effect are well represented. The last model which is based on Bouc-Wen model with mono-decreasing damping and mass element can capture the force-velocity results well in all regions. The modified Bouc-Wen model without mass element presents reasonable results when compared to the experimental once. The key advantage of this model over the other models is that, its algebraic form is suitable for system control design, because it can reproduce the behavior of the

damper with a fluctuating input voltage. The results obtained by Spencer et al [11], showed that this model is accurate in predicting damper behavior under a wide range of operating conditions. These results indicated that the modified Bouc-Wen model without mass element can be effectively used for control algorithm development and system evaluation.

#### 4. APPLICATIONS

In this section, simulation results are presented for a quarter-vehicle suspension model containing a magneto-rheological fluid (MRF) damper as shown in the Fig.17.

##### 4.1. Mathematical Model

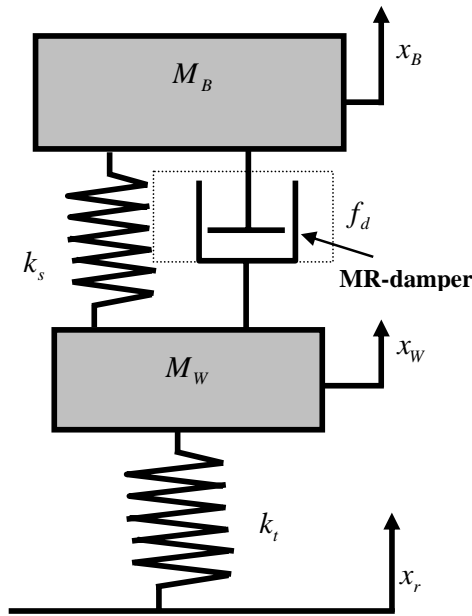


Fig.17. Quarter vehicle model with a passive MR fluid damper

The equations of motion for the shown quarter vehicle model subjected to road excitation are;

$$M_B \ddot{x}_B + k_s (x_B - x_W) + f_d = 0 \tag{20}$$

$$M_W \ddot{x}_W - k_s (x_B - x_W) - k_t (x_r - x_W) - f_d = 0 \tag{21}$$

Where the mass of the vehicle body with passenger(s) is represented by the sprung mass  $M_B$  and the mass of the wheel and associated components is represented by the un-sprung mass  $M_W$ . The vertical motion of the system is described by the displacements  $x_B, x_W$ . The excitation due to road disturbance is  $x_r$ . The suspension spring constant is  $k_s$  and the tire spring constant is  $k_t$  (neglecting the tire damping). Moreover, the damping force of the MR damper is  $f_d$ .

The MR-damper is modeled using the modified Bouc-Wen model to study the dynamic response of the quarter car model with varying volt. According to this model, the damping force corresponding to Eqs. (11) to (13) is;

$$f_d = c_1 (\dot{y} - \dot{x}_W) + k_1 ((x_B - x_W) - x_o) \quad (22)$$

Where

$$\dot{y} = \frac{1}{c_1 + c_o} [\alpha Z + c_o \dot{x}_B + c_1 \dot{x}_W + k_o (x_B - y)] \quad (23)$$

The parameter  $Z$  is calculated from the following equation;

$$\dot{Z} = -\gamma |\dot{x}_B - \dot{y}| Z |Z|^{n-1} - \beta (\dot{x}_B - \dot{y}) |Z|^n + \delta (\dot{x}_B - \dot{y}) \quad (24)$$

Where;

$$\alpha = \alpha(U) = \alpha_a + \alpha_b U \quad (25)$$

$$c_1 = c_1(U) = c_{1a} + c_{1b} U \quad (26)$$

$$c_o = c_o(U) = c_{oa} + c_{ob} U \quad (27)$$

$U$  is given by the following dynamic equation:

$$\dot{U} = -\sigma (U - v) \quad (28)$$

Where  $v$  is the voltage applied to the system. Equation (28) models the reaching rheological equilibrium of the MR fluid due to the change of magnetic field. The rate of reaching equilibrium is governed by  $\sigma$ . This model can accurately predict the behaviour of the MR-damper as it was seen in the pervious section.

A simple, conventional viscous damper modeled is used for comparison. Its exerted damping force is given by;

$$f_d = c (\dot{x}_B - \dot{x}_W) \quad (29)$$

Typical parameters of the quarter car model are chosen from Ref [13] as;

$$M_B = 240 \text{ kg}, \quad M_W = 36 \text{ kg}, \quad k_S = 16000 \text{ N/m}, \quad c = 1080 \text{ N.s/m}$$

and,  $k_t = 160000 \text{ N/m}$ .

These parameters are representative of a mid sized car.

The optimized parameters of the MR damper model were obtained by fitting the model to the experimental data by Liao [14]. A prototype MR damper (RD-1005-1 manufactured by Lord Corporation) was used to obtain the experimental data. The length of the damper is 20.83 cm in its extended position. The resulting parameters are given in Table.1 [14].

Table. 1. Parameters of the MR damper model, [14]

Parameter	Value	Parameter	Value
$c_{oa}$	784 (Ns/m)	$\alpha_a$	12441 (N/m)
$c_{ob}$	1803 (Ns/Vm)	$\alpha_b$	38430 (N/Vm)
$k_o$	3610 ( N/m)	$\gamma$	136320 (1/m <sup>2</sup> )
$C_{1a}$	14649 ( Ns/m)	$\beta$	2059020 (1 /m <sup>2</sup> )
$C_{1b}$	34622 (Ns/Vm)	$\delta$	58
$k_1$	840 (N/m)	$n$	2
$x_o$	.0908 (m)	$\sigma$	190 (1 /s)

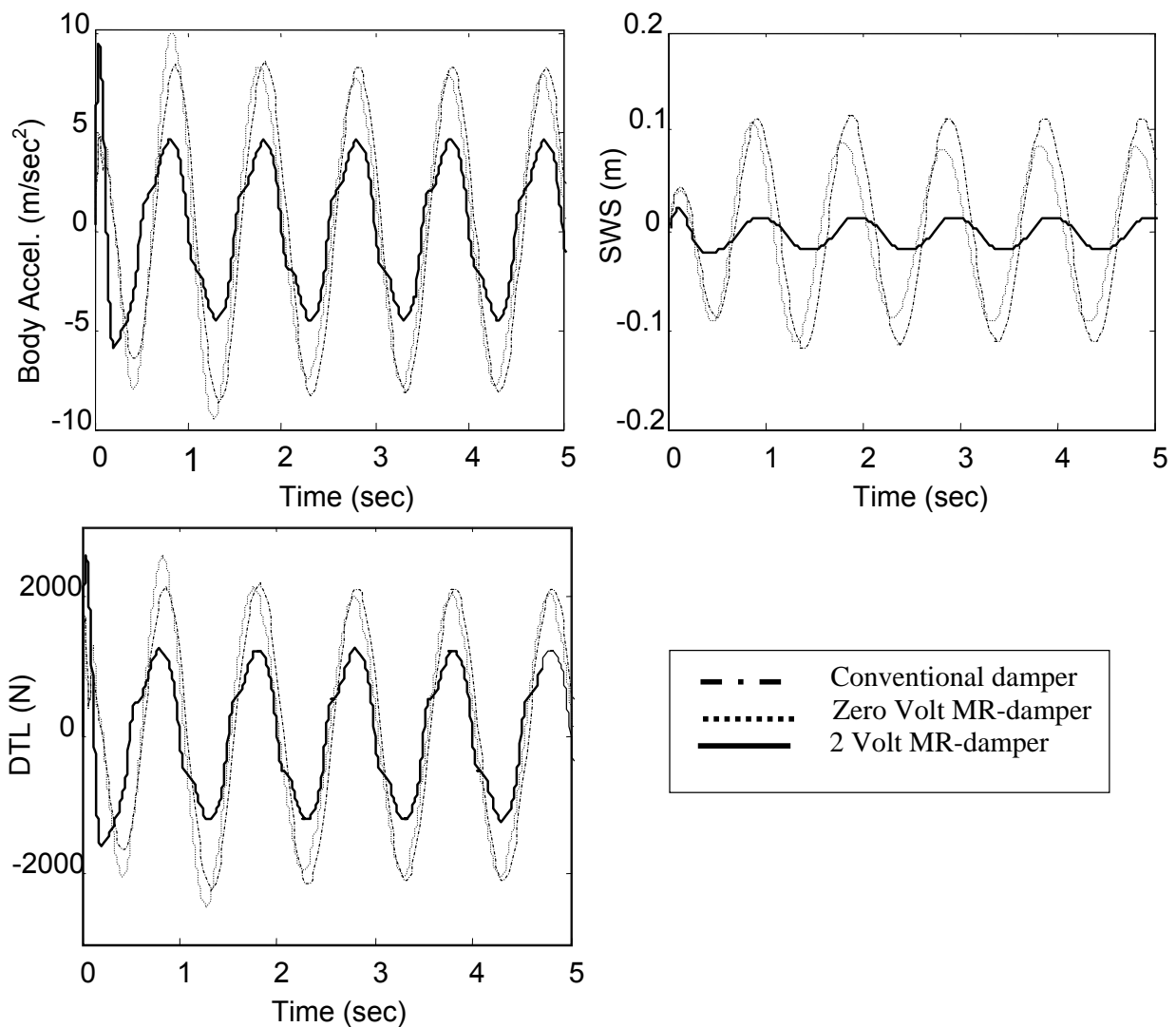


Fig.18.The body acceleration, SWS, and DTL against the time for sinusoidal excitation

Numerical results for the dynamic behavior of the model subjected to harmonic and step excitations of the vehicle wheels are obtained.

Firstly, the system response for a harmonic excitation with amplitude of 0.1 m and frequency 1 Hz are shown in the Fig.18. The figure shows the body acceleration, suspension working space (SWS), and dynamic tire load (DTL) against the time. As shown in the Fig.18, the behavior of the MR-damper at zero volt and the conventional passive damper nearly the same. As the volt applied to the MR-damper increases to 2 volt, the amplitude of the responses significantly decreases compared to the conventional passive damper.

Fig.19. shows the damping force against the damper velocity for the conventional and MR-damper. As shown, the conventional passive damper presents a purely linear relation while the MR-damper presents a non-linear behavior where the hysteretic loops are shown. Also it is shown that, as the applied volt to the MR-damper increases the damping force increases.

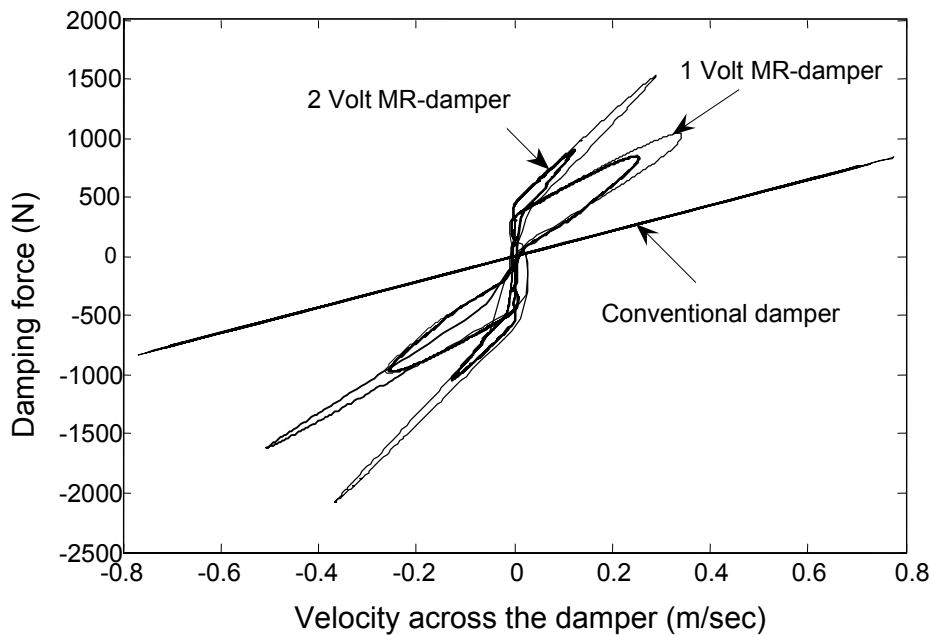


Fig.19.The damping force against the damper velocity for sinusoidal excitation

The second considered excitation is a step with height of 0.1 m at time  $t = 0$ . The corresponding numerical results are displayed in the Fig.20. As shown in the figure, the MR-damper with zero volt and the conventional passive damper show nearly the same results. Increasing the applied volt for the MR-damper to 2 volt a faster decay of the excitation especially for the SWS is achieved by the MR-damper as compared to the conventional one.

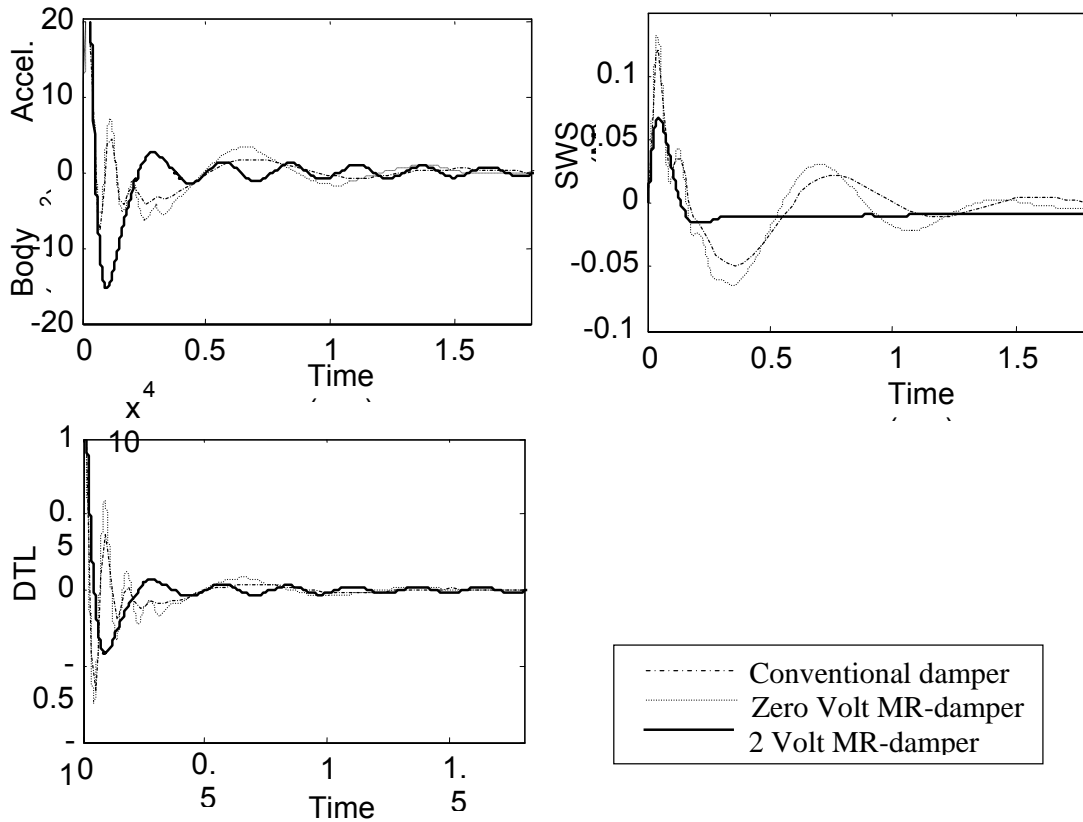


Fig.20.The body acceleration, SWS, and DTL against the time for step

### 5. CONCLUSIONS

The various possible models for electro-and magneto-rheological fluid vibration dampers have been discussed in this paper. Seven mathematical models for simulation of rheological fluid dampers have been presented. Performance of these models is compared with the corresponding published experimental results for the force-velocity and force-displacement plots. Some of these models are fitted with the experimental results in the post-yield region only, and the others are fitted with the experimental in the pr-yield and post-yield regions. By some modifications such as adding a mass to the models, or making the damping coefficient to vary with the mono-decreasing velocity function, pre-yield and post yield regions are captured well. The modified Bouc-Wen model without mass element presents reasonably results when compared to the experimental one. The key advantage of this model, over the other models, that its algebraic form is suitable for system control design because it can reproduce the behavior of the damper with a fluctuating input voltage.

Numerical example for a rheological fluid damper in a quarter-vehicle model is presented. The results showed an effect of this damper against the conventional one in ride comfort and safety of vehicles under road excitation. To fully utilize the potential of vibration control systems, rheological fluid dampers control strategies should be developed taking into consideration the controllable rheological fluid dampers.

**REFERENCES**

- [1] Mark, R. Jolly, Carlson, J., and Beth, C. Munoz, "A model of the behavior of magnetorheological materials", *J. of Smart Material and Structures*, Vol. 5, pp. 607-614, (1996).
- [2] Choi, S.B. , Choi , J.H. , Lee ,Y.S. and Han , M.S., "Vibration control of an ER seat suspension for a commercial vehicle" ,*Transactions of the ASME the journal of Dynamic systems, measurement and control*,Vol.125, pp. 60-68, (2003).
- [3] Milecki, A. and Sedziak, D., "The usage of acceleration signal to control magnetorheological fluid damper", *Int. J. of Vehicle Design*, Vol.33, Nos. 1-3, pp. 239-250, (2003).
- [4] Sims, N.D. and Stanway, R., "Semi-active vehicle suspension using smart fluid dampers : a modeling and control study", *Int. J. of Vehicle Design*, Vol.33, Nos. 1-3, pp. 76-102, (2003).
- [5] Mehdi A. and Fernando D. "A hybrid control policy for semi-active vehicle suspensions", *J. of shock and vibration*, Vol.36, No.10, pp. 59-69, (2003).
- [6] Wang, J. and Meng, G., "Magnetorheological fluid devices: Principles, characteristics and applications in mechanical engineering", *Proc. Of IMechE*, Vol.215, pp. 165-174, (2001).
- [7] Dyke, S.J., Spencer, B.F, Sain, M.K. and Carlson, J.D., "Modeling and control of magnetorheological damper for seismic response reduction", *J. of Smart Materials and Structures*, Vol. 5, pp. 565-575, (1996).
- [8] Guaugqiang Yang, " Large scale magnetorheological fluid damper for vibration migration: modeling, testing, and control", PhD Thesis, University of Notre Dame, (2001).
- [9] Stanway, R., Sproston, J. L., and Stevens, N. G., "Non linear modeling of an Electro-Rheological Vibration Damper", *J. of Electrostatics*, Vol. 20, pp. 167-184, (1987).
- [10] Hong, S.R., Choi, S.B., "Comparison of damping force models for an electroheological fluid damper ", *Int. J. of Vehicle Design*, Vol. 33, Nos.1-3, pp.17-35, (2003).
- [11] Spencer, B. F., Dyke, S. J., Sain, M. K., and Carlson, J. D., " Phenomenological model of a magneto-rheological damper", *ASCE Journal of Engineering Mechanics*, Vol.123, pp.230-238, (1997).
- [12] Wen, Y., "Method for random vibration of hysteretic systems", *J. of Engng. Mech.*, Vol. 102, pp. 219-2636, (1976).
- [13] Karnopp D., "Active suspensions based on fast load levelers ", *J. of Vehicle system dynamics*, Vol. 16, pp. 355-380, (1987).
- [14] Liao, W. H., and Lai, C. Y., " Vibration control of a suspension system Via a magnetorheological fluid damper," ; *J. of Vibration and Control*; Vol. 8, pp. 527-547, (2002).